AFRL-AFOSR-VA-TR-2019-0166

Engineering Organometallic Hybrid Perovskite/Polymer Composites for New Generation Electro-Optics Manufacturing

Zhibin Yu
FLORIDA STATE UNIV TALLAHASSEE

06/19/2019
Final Report

Air Force Research Laboratory
AF Office Of Scientific Research (AFOSR)/ RTB2
Arlington, Virginia 22203
Air Force Materiel Command

REPORT DOCUMENTATION PAGE

Form Approved
OMB No. 0704-0188

1. REPORT DATE *(DD-MM-YYYY)*	2. REPORT TYPE	3. DATES COVERED *(From - To)*
19-06-2019	Final Performance	15 Mar 2016 to 14 Mar 2019

4. TITLE AND SUBTITLE
Engineering Organometallic Hybrid Perovskite/Polymer Composites for New Generation Electro-Optics Manufacturing

5a. CONTRACT NUMBER

5b. GRANT NUMBER
FA9550-16-1-0124

5c. PROGRAM ELEMENT NUMBER
61102F

6. AUTHOR(S)
Zhibin Yu

5d. PROJECT NUMBER

5e. TASK NUMBER

5f. WORK UNIT NUMBER

7. PERFORMING ORGANIZATION NAME(S) AND ADDRESS(ES)
FLORIDA STATE UNIV TALLAHASSEE
874 TRADITIONS WAY
TALLAHASSEE, FL 32306 - 0001 US

8. PERFORMING ORGANIZATION REPORT NUMBER

9. SPONSORING/MONITORING AGENCY NAME(S) AND ADDRESS(ES)
AF Office of Scientific Research
875 N. Randolph St. Room 3112
Arlington, VA 22203

10. SPONSOR/MONITOR'S ACRONYM(S)
AFRL/AFOSR RTB2

11. SPONSOR/MONITOR'S REPORT NUMBER(S)
AFRL-AFOSR-VA-TR-2019-0166

12. DISTRIBUTION/AVAILABILITY STATEMENT
A DISTRIBUTION UNLIMITED: PB Public Release

13. SUPPLEMENTARY NOTES

14. ABSTRACT

This AFOSR funded project under award number FA9550-16-1-0124 through the Young Investigator Program, aims at replacing the perovskite thin film with a film of perovskite/polymer composite for optoelectronic devices. The composite will be advantageous for improving the processability of perovskite optoelectronics. The composite will also enhance the morphological and compositional resistance of perovskites to humid fabrication and service environments. By embedding the perovskite crystals inside a polymer matrix, the perovskites can be less toxic to handle compared to the pure perovskite film. This final project report summarized the progresses of the proposed tasks in the past three years. Overall, the PI and his team have systematically investigated the structure-process-property relationships of perovskite/polymer composites. Such studies have resulted in solution-processed perovskite LEDs with a record luminance intensity, stretchable perovskite LEDs with a 3-5 times lower turn-on voltage than previously reported stretchable polymer LEDs, and 3D printed perovskite radiation detectors that decouple photon absorption-charge collection efficiency. In addition, the PI's studies have led to answers or clues to several fundamental questions including:
1) What are the structural features of the polymer that control perovskite-polymer interactions to achieve a uniform perovskite/polymer composite;
2) What are the roles of the polymers to impact the mechanical, electrical and photonic properties and manufacturing capability of the perovskite/polymer composite;
3) Adding more complexities to the above questions due to the ionic nature of most perovskite compounds, what are the roles of ion migration in the perovskite/polymer composite affecting the electrical and photonic properties of the perovskites, and how they impact the operation stability of perovskite optoelectroni

15. SUBJECT TERMS
hybrid pervoskite, wearable electronics, polymer perovskite composite

Standard Form 298 (Rev. 8/98)
Prescribed by ANSI Std. Z39.18

16. SECURITY CLASSIFICATION OF:			17. LIMITATION OF ABSTRACT	18. NUMBER OF PAGES	19a. NAME OF RESPONSIBLE PERSON
a. REPORT	b. ABSTRACT	c. THIS PAGE			CASTER, KENNETH
Unclassified	Unclassified	Unclassified	UU		19b. TELEPHONE NUMBER *(Include area code)* 703-588-8487

Engineering Organometallic Hybrid Perovskite/Polymer Composites for New Generation Electro-Optics Manufacturing

Recently, a group of organometallic hybrid perovskite (perovskite) compounds have attracted much attention owing to their remarkable optoelectronic properties and good solubility in certain organic solvents, potentially enabling many large-area and low-cost electronic and optical devices including solar cells, light-emitting diodes (LEDs), photodetectors and chemical sensors. In most demonstrated applications, a thin layer of a perovskite film was used.

This AFOSR funded project under award number FA9550-16-1-0124 through the Young Investigator Program, aims at replacing the perovskite thin film with a film of perovskite/polymer composite. If successful, the composite will be advantageous for improving the processability of perovskite optoelectronics. The composite will also enhance the morphological and compositional resistance of the perovskite thin film to humid fabrication and service environments. Moreover, by embedding the perovskite crystals inside a polymer matrix, the perovskites can also be less toxic to handle compared to the pure perovskite film that usually has a weak adhesion with most substrates.

For such a goal, the PI and his team have systematically investigated the structure-process-property relationships of perovskite/polymer composites within the past three years. Such studies have resulted in solution-processed perovskite LEDs with a record luminance intensity, stretchable perovskite LEDs with a turn-on voltage that is 2-3 times lower than previously reported stretchable polymer LEDs, and 3D printed perovskite radiation detectors that decouple photon absorption and charge collection. In addition, our studies have led to answers or clues to several important fundamental questions including:

1) What are the structural features of the polymer that control perovskite-polymer interactions to achieve a uniform perovskite/polymer composite;
2) What are the roles of the polymers to impact the mechanical, electrical and photonic properties and manufacturing capability of the perovskite/polymer composite;
3) Adding more complexities to the above questions due to the ionic nature of the perovskite compounds, what are the roles of ion migration to affect the electrical and photonic properties of perovskites, and how they impact the operation stability of perovskite optoelectronic devices.

I. Thrust #1: Perovskite-polymer interactions and deterministic heterogenous nucleation to engineer perovskite thin film morphology

1.1 perovskite nucleation and crystallization in polymers

Thin-film processing of perovskites has been a challenge due to the formation of voids especially when they were processed in a humid environment. The scanning electron microscope (SEM) results in Figure 1 were reported by Prof. Alex Jen's group in 2015 [Yang Z. B., et. al. Advanced Energy Materials, 2015]. Even in a very dry ambient, for instance, with lower than 15% relative humidity, micrometer size pinholes still existed in a screen-printed methylammonium lead triiodide ($MAPbI_3$) film. Similar problems were also observed by other researchers using a solution-based spin coating process. To overcome such a problem, Prof. Henry Snaith's group used a thermal evaporation method in 2013, in which the organic and inorganic precursors of the perovskite were concurrently deposited in a high vacuum evaporation chamber [Liu M. Z., et al., Nature, 2013]. A Korean group used a solvent engineering method in 2014, in which a perovskite anti-solvent was introduced during the spin-coating process before the film was completely dry [Jeon N. J., et al., Nature Materials, 2014]. Both methods had shown their effectiveness to obtain very smooth and pin-hole free perovskite thin films and became two of the most frequently used approaches for fabrication of perovskite optoelectronic devices.

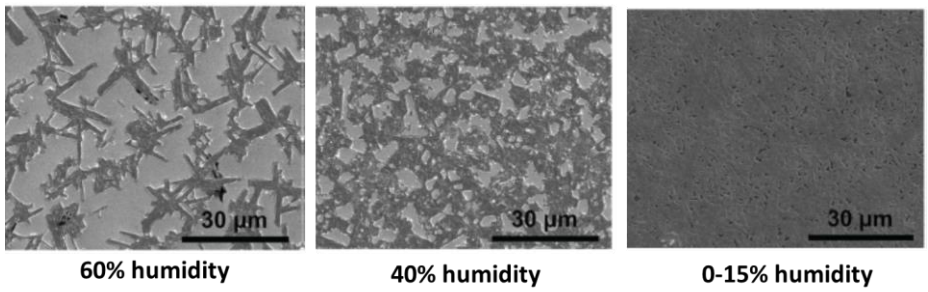

Figure 1. *SEM images of $MAPbI_3$ thin films processed at different relative humidity. a) 60-70% relative humidity, b) 40-50% and c) 15-25%.*

Alternatively, the PI has exploited perovskite/polymer composites to overcome the processing challenges. The idea was inspired by inks and pastes that are used in daily life. Many of them contain a mixture of inorganic particles and a polymer binder besides one or more aqueous or organic solvents. The polymer is essential for obtaining ideal viscosity and adhesion properties to fill up the voids among the inorganic particles and achieve a dense coating.

Compared with conventional inks in which inorganic particles (crystals) are typically synthesized beforehand, the perovskite/polymer solution initially exists in a homogenous state and the perovskite crystals are formed when the organic solvent is removed during the coating process. In principle, the incorporated polymer not only physically fills the voids among the formed perovskite crystals, it also participates in the perovskite nucleation and crystallization process; thus, the polymer can have a more direct influence on the grain size, morphology and optoelectronic properties of the resulting perovskite/polymer composite films.

In general, the nucleation density during the perovskite nucleation process can be modeled with the equation (1), where k is a unitless constant related to the capture cross section of perovskite precursors by the nucleation islands and the molecular interaction between the perovskite and the polymer; α is a positive constant less than one related to the critical nucleus size; F is the incoming "flux" of perovskite precursors that is dependent to solvent evaporation kinetics after screen printing; h roughly equals to the thickness of the perovskite thin film, and D is the diffusivity of perovskite precursors in the screen-printed film.

$$N = K.\left(\frac{Fh^4}{D}\right)^{\alpha} \qquad (1)$$

Adding a polymer to the precursor solution increases the solution viscosity, thus hindering the diffusivity of perovskite precursor at the solvent drying stage. The result is an increased nucleation density, and therefore smaller sized and more uniform perovskite crystals can be formed. It is further hypothesized that the interaction of the polymer and the perovskite crystals could also play a pivotal role for obtaining uniform perovskite/polymer composite films possibly by affecting the k and α values of equation 1.

As a proof of concept, we first examined a composite consisting methylammonium lead tribromide ($MAPbBr_3$) and polyethylene oxide (PEO). The reason of using PEO will be explained in a following session when the electronic and ionic properties of the composites are discussed. We prepared the $MAPbBr_3$/PEO composite thin films by a one-step spin coating process from a mixture solution containing the perovskite precursor (methylammonium bromide and lead (II) bromide in a 1.5 to 1 molar ratio) and PEO in dimethylformamide (DMF). The SEM images in Figure 2 manifest the morphology evolution of the composite with increasing PEO concentration. In the $MAPbBr_3$ only film, the overall coverage of perovskite on the substrate is low (~50%). This

observation agrees well with the general difficulty of processing perovskite with a solution-based process.

Instead, we found that a smooth and pinhole-free film can be readily obtained by incorporating PEO with the perovskite. As illustrated in Figure 2b-d, when the PEO concentration increases, the crystal size gets much smaller and the surface coverage greatly improves. At 0.75:1 ratio, the film becomes smoother, continuous and pinhole free.

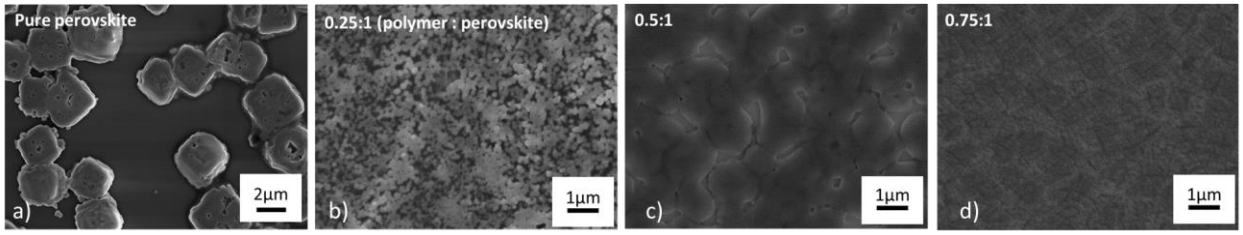

Figure 2. *SEM images of samples from spin-coating a) a methylammonium lead tribromide ($MAPbBr_3$) film, and b)-d) $MAPbBr_3$/polyethylene oxide (PEO) composite films with PEO/ $MAPbBr_3$ ratio of 0.25:1, 0.5:1, and 0.75:1, respectively.*

Adding PEO also helped realize uniform and dense perovskite/polymer composite films with a screen-printed process even at a highly humid environment, as shown by our experimental results in Figure 3.

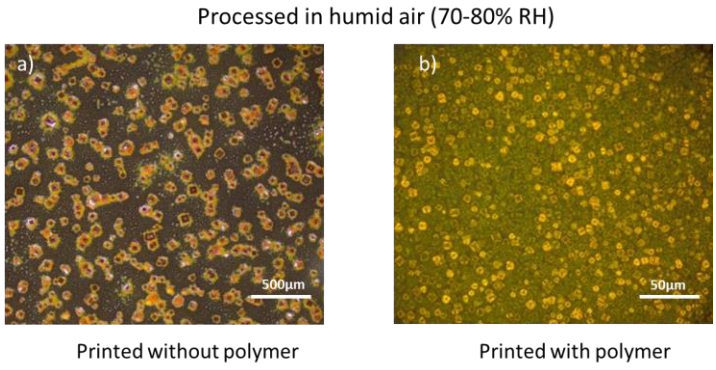

Figure 3. *Optical microscopic images of screen-printed a) $MAPbBr_3$ (Scale bar: 500 μm) and b) $MAPbBr_3$/PEO (Scale bar: 50 μm).*

High molecular weight (Mw > 600,000) PEO worked well for uniformly dispersing $MAPbBr_3$, however it failed for inorganic perovskite including $CsPbBr_3$ and inorganic double perovskite ($Cs_2AgBiBr_6$) etc. We speculated it was likely due to a lower solubility of the CsBr (AgBr and $BiBi_3$) in PEO. Since the inorganic perovskites or double perovskites usually exhibit a

high structural and temperature stability compared to their organic perovskite counterparts that are desired for device applications, it is meaningful to investigate new polymers that can disperse these perovskites into uniform and dense composite films; equally important, to answer the question what are the structural features of the polymer that influence the nucleation and crystallization kinetics of inorganic perovskite in polymer.

Polar protic solvents are often used to dissolve inorganic salts. It is hypothesized polymers that contain similar structure features, for instance, with hydroxy groups or amine groups can help disperse inorganic perovskite more uniformly. We first used $Cs_2AgBiBr_6$ as one example and designed a series of experiments to test this hypothesis. As shown in Figure 4, $Cs_2AgBiBr_6$ films without and with a PEO polymer were obtained by dropping a mixture solution on a glass substrate and allowing the solvent (dimethyl sulfoxide, DMSO) to evaporate at 80 °C. From Figure 4b to 4d, the PEO polymers had different molecular weights of 1,000,000, 600,000, and 100,000, respectively. It is observed the composite film became much more uniform when a lower molecular weight PEO was used. It is explained that the PEO with a lower molecular weight exhibits a higher concentration of hydroxyl groups locating at both ends of each polymer chain.

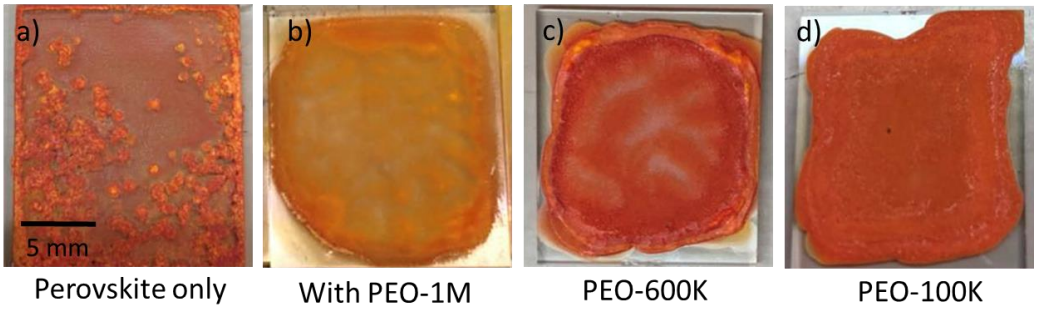

Figure 4. *Photos of a) $Cs_2AgBiBr_6$ and b)-d) $Cs_2AgBiBr_6$/PEO (weight ratio 2:1) composite films with different PEO molecular weights (1,000,000, 600,000, and 100,000).*

In comparison, poly(methyl methacrylate) (PMMA) polymers with different molecular weights all showed poor film uniformity similar to Figure 5a. Such a finding demonstrates that the resulting film morphology is mostly independent on the molecular weight of the polymer if no hydroxyl groups are incorporated. However, if the PMMA is modified with side chains containing hydroxyl groups ((poly(2-hydroxyethyl methacrylate), PHMA), greatly improved film uniformity could be achieved (Figure 5b). We also tested polyvinyl alcohol (PVA). The film uniformity was as good as the PHMA (Figure 5c). Again, the results proved the important role of the hydroxyl

groups in polymer producing homogenous halide perovskite/polymer composites. It is worth noting that the concentration of hydroxyl groups in the polymer is also important for dispersing $CsPbBr_3$. As observed in our experiments, $CsPbBr_3$/PEO formed a uniform film when the PEO molecular weight was at or below 100,000 and formed a non-uniform film when the PEO molecular weight was above 100,000.

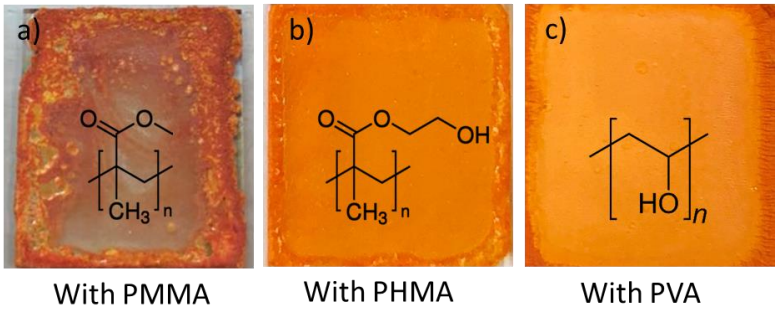

Fgure 5. *Photos of $Cs_2AgBiBr_6$/polymer (weight ratio 2:1) composite films with different polymers. a) PMMA, b) PHMA, and c) PVA.*

Other than hydroxyl containing polymers, polyvinylpyrrolidone (PVP) was also found effective in dispersion both $CsPbBr_3$ and $Cs_2AgBiBr_6$. As shown in Figure 6, mixing the $CsPbBr_3$ with PEO did not produce a continuous film. In contrast, the $CsPbBr_3$ can be well dispersed by PVP with a much finer grain size and grain size distribution. It is likely that the pyrrolidone group in the PVP increased the solubility of the inorganic perovskites like the function of hydroxyl groups due to a high polarity of the pyrrolidone and a lone pair electron in the nitrogen atom.

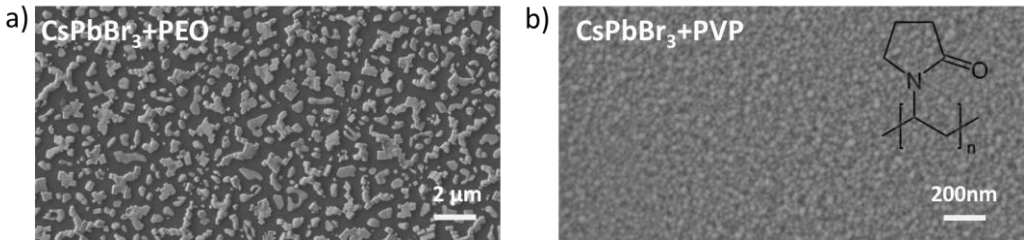

Figure 6. *SEM images of CsPbBr3/polymer composites. a) with PEO and b) with PVP.*

Aided by the current understanding of perovskite and polymer interactions, we have realized uniformly dispersed perovskites in polymer matrices and successfully applied these composite films for LEDs and X-ray detectors during the funding period of this AFOSR project. More device application work will be elaborated in the 2nd thrust of discussing the mechanical, electronic and photonic properties of the composite. The example below briefly highlights the role

of using polymers to fine-tune the morphology of $CsPbBr_3$ thin films and realizing the brightest perovskite LEDs with an ultra-low turn-on voltage.

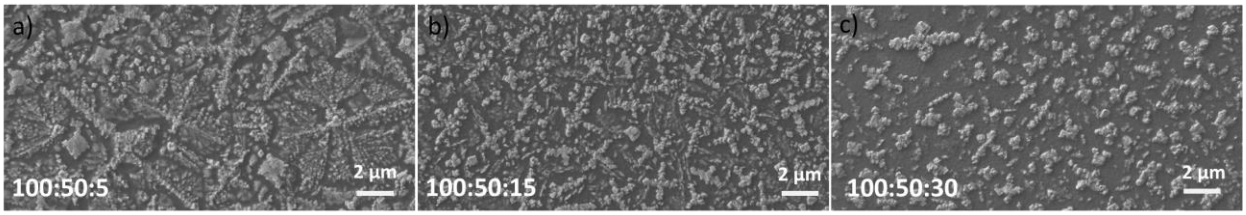

Figure 7. *SEM images of $CsPbBr_3$/PEO/PVP composites with weight ratios of a) 100:50:5, b) 100:50:15, and c) 100:50:30*

As observed in Figure 6, $CsPbBr_3$ forms a non-continuous film with a larger grain size in PEO, however forms a dense and uniform film with a much smaller grain size in PVP. A continuous film is critical for LEDs since pinholes can create electrical short and greatly reduce the electroluminescence efficiency. Nonetheless, crystals with a small grain size trend to be embedded into the polymer and can increase electrical contact resistance to the electrodes. Thus, we used a polymer blend of high molecular weight PEO and PVP to optimize the morphology of the $CsPbBr_3$ crystals in our experiments. It was discovered with a mixing weight ratio of 100:50:5 ($CsPbBr_3$:PEO:PVP), the composite film was fully continuous and perovskite crystals were nearly all exposed (Figure 7a). With increased PVP concentration, the areal coverage of exposed perovskite crystals was reduced (Figure 7b, c). In principle, a lower molecular weight PEO can replace the PVP for film morphology optimization. However, an excessive concentration of hydroxyl groups in the composites was found to decrease LED stability and performance, thus was avoided for LED applications.

With this optimized film morphology, we achieved ultra-bright perovskite LEDs with a low turn-on voltage. The LEDs were constructed with an indium tin oxide (ITO) anode, $CsPbBr_3$-PEO-PVP composite emissive layer, and indium-gallium eutectic (In-Ga) cathode without intentionally employing an electron injection layer (EIL) or hole injection layer (HIL). Such single-layer devices start emitting green light at 1.8-1.9 V, reach a maximum luminance of about 600,000 cd m^{-2} at 4.9 V and a power efficiency about 15 lm W^{-1} (Figure 8a-c). Noticeably, the maximum luminance intensity is about 9 times of the previous record in $MAPbBr_3$ LEDs and 11 times of $CsPbBr_3$ LEDs.

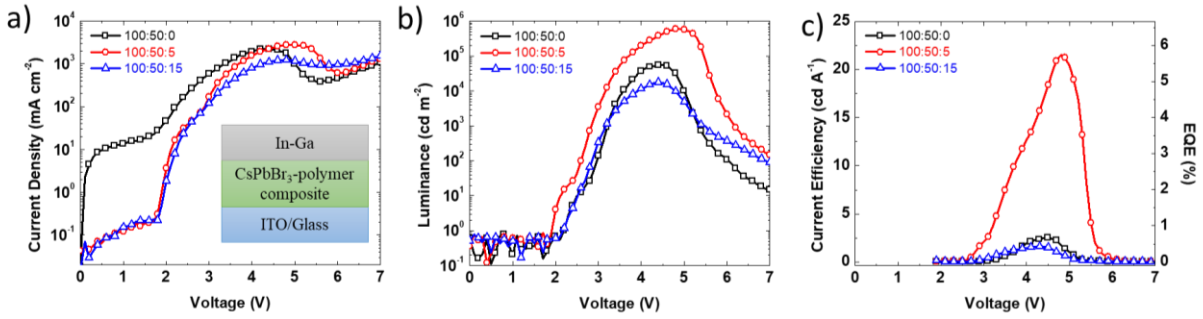

Figure 8. *a) Current density, b) luminance, and c) current efficiency/external quantum efficiency (EQE) versus voltage characteristics of the $CsPbBr_3$/PEO/PVP LEDs with different PVP compositions in the emissive layers. The inset in a) shows the LED device structure as "ITO anode/$CsPbBr_3$-polymer composite/In-Ga cathode".*

It is worth mentioning that our LEDs has been winning in both high brightness and low turn-on voltage over all perovskite-based LEDs worldwide since we first reported our results in 2016. Our device was also one of the champions in power efficiency from 2016 to 2018. However, with the intensive investments among Europe and Asian countries in perovskite LEDs, our efficiency record had been surpassed by a few research groups that have recently reported perovskite LEDs with EQE of >20%. All these devices are based on a multilayer device structure including layers of electron injection materials and hole injection materials to balance electron and hole concentrations in the emissive layer. The PI recently has submitted a DURIP proposal to AFOSR for purchasing an integrated glovebox and material evaporation system. With this add-on, the PI can take the advantage of the multilayer device structure to obtain a high EQE; meanwhile maintaining the low operation voltage of the composite film to achieve an even higher power efficiency than the European and Asian groups.

1.2 heterogenous nucleation and perovskite thin film growth

In addition to study the perovskite-polymer interactions, the PI also explored how perovskites interacted with different substrates and investigated their nucleation and growth kinetics for thin film formation on engineered heterogeneous substrates.

In general, the probability a site nucleates is given by an Arrhenius relationship (equation 2), where A is a prefactor and G* is the nucleation barrier energy. G* is sensitive to the surface

chemistry of the substrate. Thus, the nucleation densities can be varied in large magnitudes depending on the substrate choices.

$$P(N) = Aexp\left(\frac{-\Delta G^*}{k_b T}\right) \quad (2)$$

To verify this hypothesis for perovskite crystallization, we studied perovskite thin film growth on thermally evaporated molybdenum oxide thin films, E-beam evaporated gold (Au) thin films and silicon oxide-silicon substrates. Figure 9 shows the perovskite on the molybdenum oxide exhibited a much smaller grain size average (~ 500 nm) than on the gold film (~10 μm) and silicon oxide (~200 μm), suggesting a large difference of nucleation barriers for the three substrates with the molybdenum oxide being the lowest and the silicon oxide being the highest. It is believed the high density of crystalline defects and dangling bonds on the molybdenum oxide and gold surfaces have served as nucleation promotors/catalysts for perovskite crystallization.

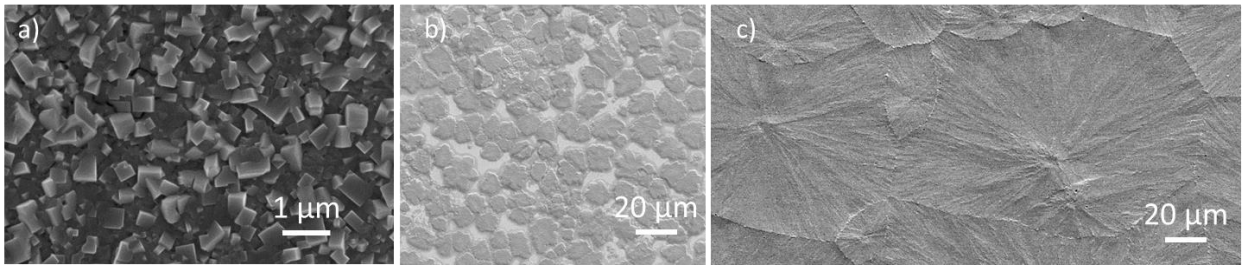

Figure 9. *SEM images of perovskite films grown on a) molybdenum oxide, b) gold continuous thin films and c) bare SiO_2/Si substrate.*

With the findings in Figure 9, we engineered a silicon oxide-silicon substrate with periodically patterned Au islands. By spinning a solution containing the halide perovskite precursors, halide perovskite crystals were found to nucleate on the Au islands and grow outwards onto the bare SiO_2/Si area until neighboring crystals met and merged into a continuous film. The size of individual grains was eventually determined by the separation distance (pitch size) between neighboring Au islands. As shown in Figure 10, grains in ordered arrays and with faceted shapes are obtained. The sizes of the grains are very uniform and exactly duplicate the pitch size of the gold arrays, suggesting the nucleation of all the perovskite crystals had only occurred at each gold island. Such a deterministic growth mode has been successfully applied to $MAPbI_3$, $MAPbBr_3$, $CsPbBr_3$ and the various ternary alloys with a uniform grain size as large as 500 μm throughout the film.

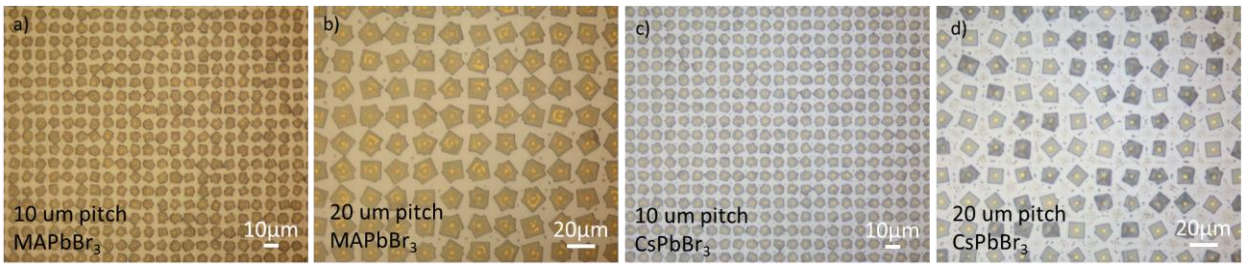

Figure 10. *Deterministic nucleation and crystal growth of $MAPbBr_3$ on patterned $Au/SiO_2/Si$ substrates with a) 10 μm and b) 20 μm pitch sizes, and the growth of $CsPbBr_3$ crystals on patterned $Au/SiO_2/Si$ substrates with c) 10 μm and d) 20 μm pitch sizes.*

To date, most reported perovskite solar cells and LEDs employed a polycrystalline thin film for light absorbing or light emitting purposes. The size of grains in such films typically varied from sub-100 nanometres to a few micrometres. The high density of grain boundary defects can trap charge carriers and aid the diffusion of water molecules and ionic species in the perovskites, deteriorating their structural integrity and electrical properties in long-term applications.

The large grain sizes of our perovskite thin films from the deterministic nucleation process were found beneficial to restrict ion migration processes in perovskites, leading to photodetectors with a low dark current and a high on/off ratio under a constant bias, and without hysteresis under a dynamic bias. The large grain also enhanced the stability of the halide perovskite thin films in ambient environments. Minimal structural or morphological damages were seen in all the perovskites after six-month exposure in humid air (50-70% relative humidity).

Moving forward, it is possible to apply this deterministic growth process for controlling nucleation and crystal size and distribution in perovskite-polymer composites. For instance, the nucleation catalysts in colloidal nanoparticle forms can be uniformly dispersed in the perovskite-polymer precursor solution. The colloidal nanoparticles will be eventually embedded inside the fully-grown perovskite crystals. Since the size of the particles (a few nanometers) is small compared to the expected perovskite crystal size (100 nanometers and above), the electronic properties of the catalysts may not largely affect the perovskites. In this way, the size of the perovskite crystals can be tuned more precisely by adjusting the concentration of the colloidal particles. A one-pot synthesized perovskite-polymer composites with different crystal sizes can be very interesting for studying the fundamental effects of grain sizes on charge transportation, ion migration and device stability characteristics of perovskite/polymer composites.

II. Thrust #2: mechanical, electrical and photonic properties and new manufacturing perspectives of perovskite/polymer composites

2.1 new mechanical properties enabled by perovskite/polymer composites

In addition to the advantage of tuning the morphology of perovskite thin films, using perovskite/polymer composites can also improve their mechanical properties. Since halide perovskites are mostly ionic compounds, they are very fragile and not ideal for flexible devices especially when a relatively large film thickness is required, for instance, in X-ray detectors. In contrast, highly flexible or even stretchable perovskite optoelectronics are possible if perovskite/polymer composites are used to replace the pure perovskite films.

From the previous studies of perovskite-polymer interactions and morphology, micrometer size perovskite crystals could be formed that were partially embedded in a polymer matrix. With this composite microscopic structure, it is hypothesized that the polymer matrix can serve as a microscale flexible connector for the rigid and brittle perovskite microcrystals and induces highly flexibility or even stretchability to a perovskite/polymer composite thin film. As a proof of concept, we tested the mechanical properties of a $MAPbBr_3$/PEO composite film, where the PEO has a molecular weight (Mw) of 5,000,000. Since PEO has a glass transition temperature (Tg) of around −67 °C, a high molecular weight can enhance the elasticity of the polymer at room temperature due to a strong polymer chain entanglement.

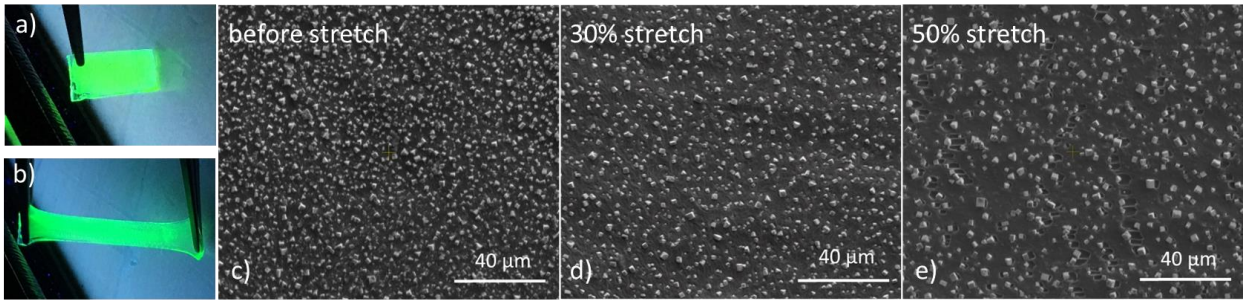

Figure 11. *Photos of the $MAPbBr_3$/PEO composite film under 365nm UV irradiation a) before stretching, and b) after stretching to ~100% strain. (c) SEM images of the $MAPbBr_3$/PEO composite thin film before stretching, (d) after stretching to 30% strain, and (e) to 50% strain.*

Figure 11 a and b show photos of a $MAPbBr_3$/PEO composite film on an elastic polydimethylsiloxane (PDMS) substrate under 365nm UV irradiation. The film appeared

homogeneous even after the composite film was elongated with about 100% linear strain. The surface morphology of the $MAPbBr_3$/PEO composite thin film was characterized with SEM. Without stretching, the top view SEM image shows a dense arrangement of perovskite crystals partially embedded into the PEO polymer matrix (Figure 11 c). The gaps between the crystals are filled by the polymer and a pin-hole free film is obtained. At 30% linear strain, the polymer elongates along with the PDMS substrate and a reduction in perovskite density is observed (Figure 11 d). At 50% strain, the density of the crystals further decreases and tearing of the polymer matrix by the perovskite can be seen in certain locations (Figure 11 e) suggesting the upper stretching limit was reached for this $MAPbBr_3$/PEO composite film. It is evident that mixing a polymer has greatly improved the mechanical properties of perovskite thin film and a maximum of 50% uniaxial strain in the $MAPbBr_3$/PEO composite has already exceeded the deformation requirement for wearable device applications. Nonetheless, we believe the stretching limit can be further extended by a systematic study of how different polymer structures will impact the adhesion at the perovskite/polymer interface.

We continued to fabricate stretchable LEDs with the $MAPbBr_3$/PEO composite film as the light emitter, a PEO modified poly(3,4-ethylenedioxythiophene) polystyrene sulfonate (PEDOT:PSS) as a transparent and stretchable anode, and In-Ga as the cathode. As shown in Figure 12a and b, the as-prepared devices emitted visible green light starting at 2.4 V. The luminance intensity increased with voltage and obtained a value of 15,960 cd m^{-2} at 8.5 V. The current efficiency also showed a rising trend with applied voltage and saturated at 2.7 cd A^{-1} after about 5.2 V, corresponding to a maximum EQE of 0.62%. Stretching had no effect on device turn-on voltage and even increased the device current efficiency. At 20% uniaxial strain the devices obtained a value of 10,148 cd m^{-2} at 8.5 V, and a saturation efficiency of 2.9 cd A^{-1} after 4.9 V. At 40% strain, a luminance peak of 7,340 cd m^{-2} and an efficiency maximum of 3.2 cd A^{-1} were both observed at 7.7 V. We tend to believe the slight increase of device efficiency is caused by a more balanced electron/hole recombination due to a reduced emissive layer thickness in the stretched device. It is worth noting the luminance intensities and operating voltages in our devices are by far the best among all reported intrinsically stretchable LEDs. For instance, the PI reported the first intrinsically stretchable polymer LEDs (PLEDs) when he was a Ph.D. student in Prof. Qibing Pei's group at UCLA. The LEDs emitted blue light and could be stretched by 45%, turning-on at 4.5 V and reaching 300 cd m^{-2} at 12 V [Yu Z. B., et al. Advanced Materials, 2011]. The PI's colleague

then Liang *et al.* achieved green color stretchable LEDs that were capable of more than 100% maximum strain [Liang J. J., et al. Nature Photonics, 2013]. The devices turned-on at 6.8 V and reached about 2,200 cd m^{-2} at 21 V.

Figure 12c and d show the before and after strain photos for an illuminated LED. The devices emitted a uniform green light even after 40% linear strain. Furthermore, the stretchable perovskite LEDs presented in this work can withstand repetitive stretching cycles between 0-40% strain. No catastrophic degradation of illumination uniformity and intensity occurred after 100 testing cycles between 0-40%, further demonstrating the compliance and robustness of the stretchable devices.

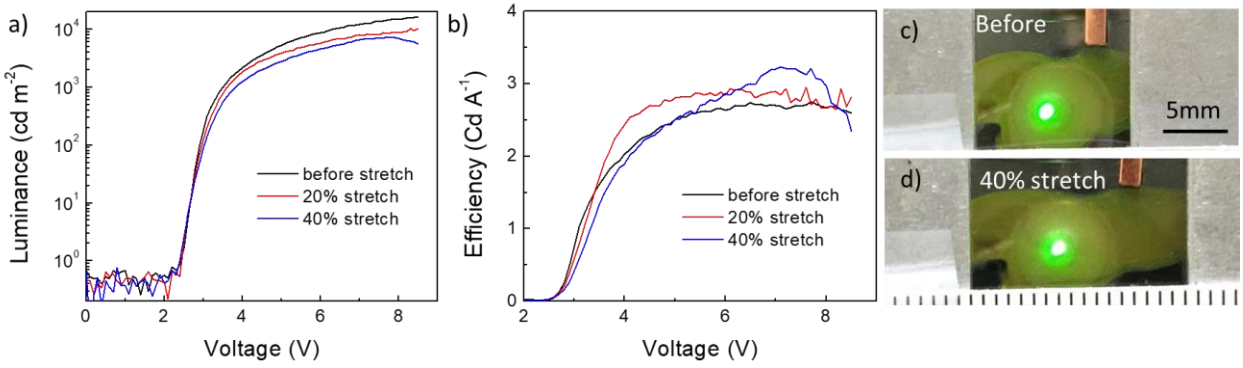

Figure 12. *a) luminance-voltage, and b) current efficiency-voltage characteristics of the stretchable perovskite LEDs before and after stretching to 20% and 40% strain. c-d) Photos of a lit LED under a 4 V bias before (top) and after (bottom) stretching to 40% strain.*

This work represents an imperative stride in the field of perovskite electronics by opening new possibilities towards devices that can tolerate very high deformation using perovskite/polymer composites. For instance, stretchable perovskite solar cells can be made leveraging this approach. For this purpose, the $MAPbBr_3$ will be replaced with $MAPbI_3$ for effective absorption of sun light. An exploration on stretchable materials is also critical for electron transport in the stretchable perovskite solar cells.

2.2 new manufacturing methods enabled by perovskite/polymer composites

The improved mechanical properties of perovskite/polymer composites can also innovate the manufacturing processes of perovskite electronics. Many traditional and emerging manufacturing methods for polymer and composite manufacturing can now be used to process

perovskite/polymer composites including hot pressing/molding, melt extrusion or even 3D printing etc. The perovskite/polymer can also be made into different shapes including sheets, plates and filaments etc. as shown in Figure 13 a-e. Such samples remained the luminescent property (Figure 13 b and e) and crystallinity (Figure 13f) of perovskites and overall plasticity of polymers (Figure 13g).

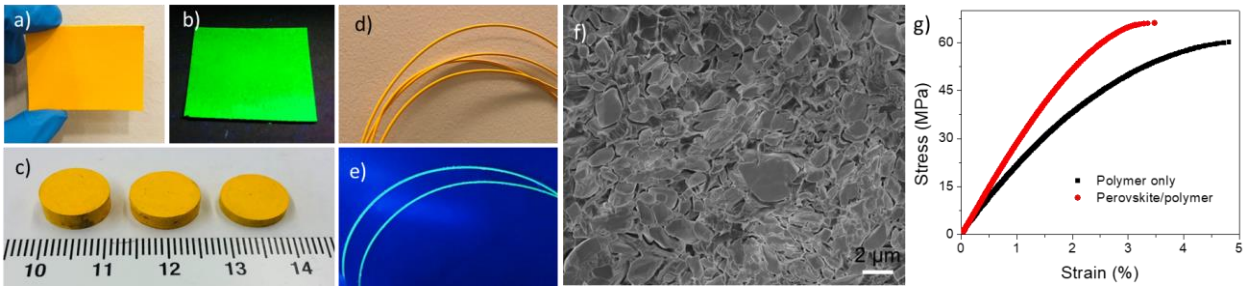

Figure 13. *Processing $CsPbBr_3$/polymer composites into different forms with different manufacturing methods: a) a hot-pressed sheet in ambient light and b) under 365nm UV light. c) melt-molded composite plates with different thicknesses. The polymer used in a-c was polyvinylidene difluoride (PVDF) mixed with some PEO. d) hot extruded composite filaments (about 2mm diameter) in ambient light and e) under 365nm UV light, and f) a SEM image showing the cross-sectional view of the filament. The polymer used in d-f was polylactic acid (PLA), a common thermoplastic polymer for 3D printing. g) stress-strain characteristics of $CsPbBr_3$/PLA (2:1) and PLA (manuscript submitted).*

While perovskite thin films with thicknesses from tens of nanometers to a few micrometers are useful for solar cells and LEDs, the thick samples shown in Figure 13 can be used for radiation detectors where high energy photons won't be effectively absorbed if sample thickness falls below tens of micrometers for X-ray (about 30 keV) or a few mm for gamma ray (about 500 keV). In the same time, it is important to characterize the charge transport properties of the perovskite/polymer composite. One fundamental question is whether the charge carriers can be collected within the thickness range that is required for absorption.

2.3 charge carrier transportation of perovskite/polymer composites

The charge carrier drifting length of the $CsPbBr_3$/PLA (2:1) composite was measured using an experimental design as shown in Figure 14a. Fullerene C60 (C_{60}) and MoO_x were thermally evaporated as n-type and p-type selective contacts to the perovskite composite, respectively. The

thicknesses of the composites were varied from 50 µm to 500 µm. Due to a high absorbance of $CsPbBr_3$ to 480nm blue light, it is expected the penetration of incident photons will be limited within about 100nm depth from the Au surface, which is negligible compared with the thicknesses of the measure composite samples. Current density-electrical field characteristics were measured with light on and off for samples with different thicknesses as shown in Figure 14 b, c. A summary plot of net photocurrent is shown in Figure 14d. The net photocurrent for samples with different thicknesses under the same electrical field can be simulated using equation 3, where A is a prefactor, B is a constant to correct systematic measurement errors, and Ƭ is charge carrier drifting length. Following this equation, a charge drifting length of about 80 µm is obtained at an electrical field of 400 V mm^{-1}.

$$Photocurrent = A * exp(-sample\ thickness/\tau) + B \qquad (3)$$

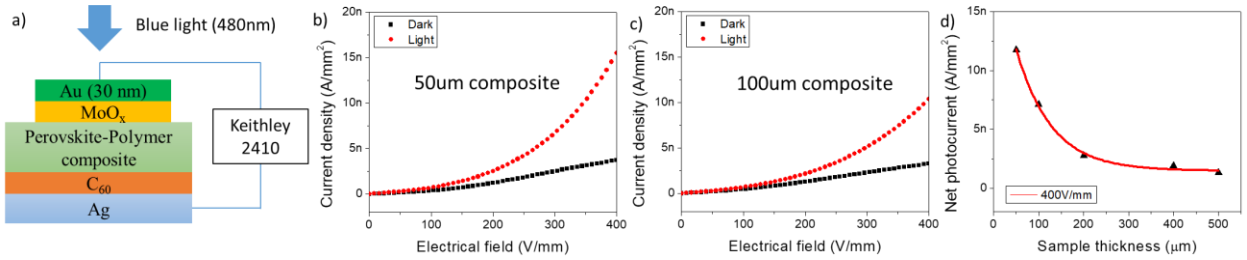

Figure 14. *a) an experimental setup and device structure for measuring charge carrier drift length of $CsPbBr_3$/PLA (2:1) composites. b) and c) are current density vs. applied electrical field measured both in dark and with 480nm light for 50 µm and 100 µm composites, respectively. d) shows a summary of net photocurrent (light current minuses dark current) at 400 V mm^{-1} for composites with different thicknesses (Triangle dots are experimental data points and red solid line is a simulation curve) (manuscript submitted).*

The penetration depth is calculated to be about 200 µm for 30-50 keV (medical imaging) X-ray photons and a few millimeters for 500 keV gamma ray photons that both exceed the charge carrier drifting length of current perovskite/polymer composite. One effective way to increase the drifting length is to increase the perovskite volume ratio to the polymer, so there will be more pathways for charge carrier collection. However, this increase can sacrifice the mechanical properties of the composite. To decouple the high energy photon absorption and charge carrier collection, we proposed tandem structured radiation detectors. Given the superior mechanical

properties and tunable rheological properties of the composite, the tandem devices can be fabricated using a 3D printing process (Figure 15a). The thickness of the 3D printed film is currently limited to about 100 μm with our 3D printers. The tandem devices used 3D printed carbon/PLA as the top, bottom and interlayer connection electrodes (Figure 15 b, c). As shown in Figure 15d, with the same applied voltage, the photocurrent under the same intensity of X-ray irradiation had more than doubled in the two-layer tandem device (~ 28 nA at 40 V) compared to the one-layer device (~12 nA at 40 V). In contrast, a one-layer device with double film thickness had a current of ~ 6 nA at 80 V. The result here clearly demonstrates the effectiveness of a tandem device structure in decoupling photon absorption and charge carrier collection to improve the responsivity of high energy photon detectors. This approach can be further explored for detection of even higher energy photons in future.

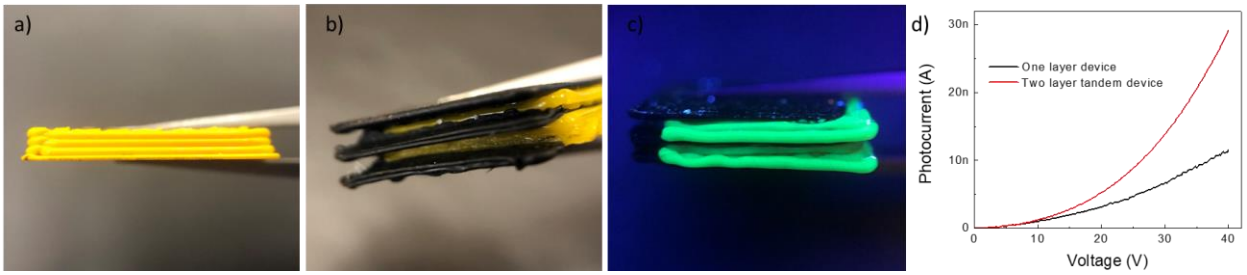

Figure 15. *a) a side-view photo of a four-layer stack of 3D printed perovskite/polymer composite, b) a side-view photo of a 3D printed tandem X-ray detector device with two layers of perovskite/polymer composites for X-ray absorption and three layers of conductive carbon/polymer electrodes, and c) a photo of the tandem device under 365nm UV light. d) Photocurrent-voltage characteristics of a one-layer device and a two-layer tandem device under X-ray irradiation (manuscript submitted).*

III. Thrust #3: roles of ion migration in the perovskite/polymer composites and perovskite single crystals

3.1 ion migration can induce doping and junction formation in perovskites even at a voltage lower than the E_g/e of perovskites

Halide perovskites are ionic compounds. It has been reported that the cations and anions in perovskites can migrate under an internal (in solar cells) or external (in LEDs) electrical field, causing severe hysteresis in dynamic measurements and device instability in long term

applications. This part of work addresses some fundamental questions including how ion migration will affect the electronic and photonic properties of the perovskites, and how it is correlated to the operation lifetime of perovskite LEDs, and how this process can be impacted by incorporating different polymers.

To study the effect of ion migration on the electronic and photonic properties of perovskite, an experimental setup as shown in Figure 16a was used. A 10 µm-thick $MAPbBr_3$/PEO film was sandwidged between an ITO bottom electrode and a carbon foam electrode. The high thickness slowed down the ion migration process and its temporal evolution could be easily observed. The carbon foam was mechanically pressed onto the composite film. This method of making electrical contact was found much better compared to thermal evaporation due to a large surface roughness of the thick composite film. The sample was placed on a heat-cooling stage to control sample temperature from 300 K to 77 K. The heat-cooling stage has an optical feedthrough for photovoltaic and photoluminescence measurements of the composite film.

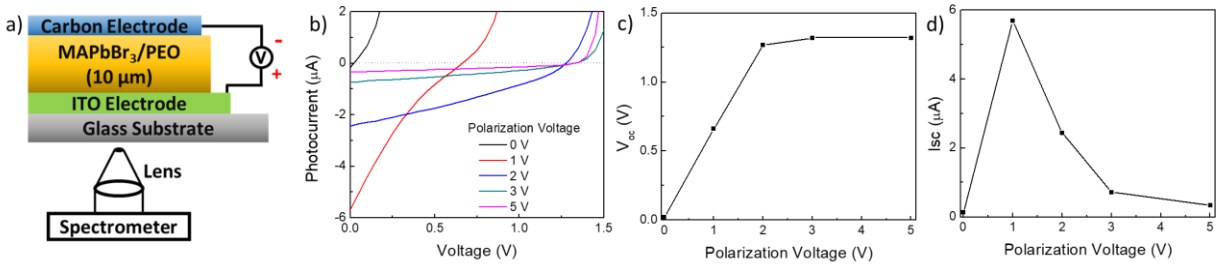

Figure 16. *a) an experimental setup to measure the photovoltaic and photoluminescence characteristics of the composite film, b) photovoltaic measurements at 77 K showing the photocurrent-voltage characteristics of the same sample after it was biased at a desired voltage (polarization) at room temperature, c) a summary of open-circuit voltage (V_{oc}) and d) short-circuit current (I_{sc}) of the composite film after each polarization at different voltages (manuscript submitted).*

When an external electrical field is applied on perovskites, anions in the perovskites move towards the anode side and cations move to the cathode side, leading to an anion-rich region at the anode/perovskite interface and a cation-rich region at the cathode/perovskite interface, respectively. In conventional inorganic semiconductors, eg. silicon, external dopants dissociate into ionized space charges and mobile charge carriers. Positive space charges (cations) go along

with free electrons and lead to a n-type doping. Negative space charges (anions) go along with free holes and lead to p-type doping. The very first question is whether ion migration/accumulation would cause n-type and p-type doping in perovskites at the cathode and anode interfaces, respectively.

We measured the photovoltaic characteristics of the composite film after it was polarized at a desired voltage for one minute at room temperature. The polarization process used here is like a charging process in lithium ion batteries (ion intercalation) or electrochemical capacitors (electrical double layers). At room temperature, the accumulated ions at the anode and cathode interfaces can provide an open-circuit voltage even without a light illumination. This will interfere the photovoltaic measurements. Such an interference can be overcome by cooling down the film to liquid nitrogen temperature (77 K) when the ions are frozen and the V_{oc} in dark becomes negligible. Thus, for each measurement, the standard operation procedure is first polarizing the composite film with a desired voltage at 300 K and followed by immediately cooling the composite to 77 K with the polarization voltage. This voltage is then removed when the temperature reaches 77 K.

As shown in Figure 16 b and c, the pristine device has a negligible V_{oc} (0.02 V) under light illumination, which is reasonable given that the high work function of cathode electrode (carbon) and the large thickness of the composite film. The V_{oc} increased to 0.66 V after 1 V polarization with the carbon electrode as cathode (-) and ITO as anode (+) and to 1.27 V after 2 V polarization. The V_{oc} then remained nearly the same with the polarization voltage increasing to 5 V. In contrast, I_{sc} largely increased after the 1 V polarization, however, exponentially decayed with further increasing polarization voltage.

PL spectra were also collected at 77 K after the composite film was polarized at different voltages. As shown in Figure 17 a and b, the PL intensity had an exponential decrease tendency with increasing polarization voltage. Moreover, the PL peak positions monotonically shifted towards short wavelengths with increasing polarization voltage. After 5 V polarization, a total blue-shift of about 22 nm was observed comparing to the non-polarized pristine composite film. The pristine film did not generate light emission at 77 K even with a 10 V bias. In contrast, the film after 5 V polarization started to emit green light at 2.5 V. This voltage is very low given the large film thickness of 10 μm. Light emission became more intense with a higher bias (Figure 17

c-f). The light emission was not uniform especially at a low bias. This is likely due to some non-uniformity of film thickness and/or carbon foam attaching. Nonetheless, this non-uniformity shouldn't affect the photovoltaic measurements since the best-performing regions usually the brightest spots in the LEDs would dominate the photovoltaic signal. The excitation laser was also focused on the bright spots for PL measurements. It is worth to mention that due to the strong absorption of the perovskite to 488 nm excitation light, the PL signal mostly came from the part of film close to the ITO electrode, which was positively biased during the polarization process for the measurements in both Figure 16 and Figure 17. So, the obtained spectroscopic data carry information of the p-doped perovskite if doping occurs.

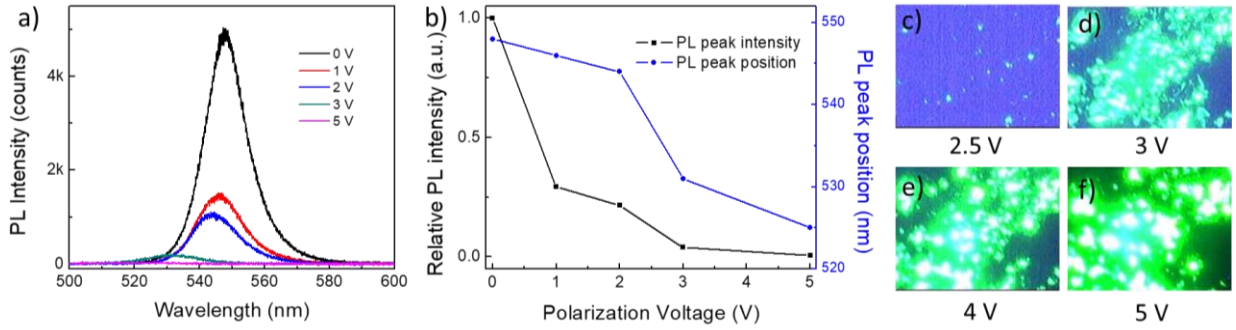

Figure 17. *a) Photoluminescence spectra measured at 77 K, b) a summary of PL intensity and peak position of the composite film after each polarization at different voltages, c-f) show photos of the sample at 77 K lit with a specified bias (manuscript submitted).*

The enhancements in V_{oc}, decreases in PL intensity and PL position blue-shifting, and efficiency light-emission turn-on all indicate that the ion migration in perovskite had caused n-type and p-type doping of the perovskite and a p-i-n junction in the perovskite. The doping and junction formation had occurred even with 1 V polarization bias, which is much lower than the bandgap of the perovskite (2.2-2.3 eV). The very large shift of PL position after 5 V polarization indicates a heavily p-doped perovskite region had likely formed. The first increase in I_{sc} was attributed to the p-i-n junction formation and V_{oc} increase. The subsequent I_{sc} decrease was explained by the decrease in PL intensity, as light absorption and charge carrier generation occurred in this heavily p-doped region, non-radiation recombination had greatly reduced the carrier collection efficiency.

The same measurements were repeated, on the other hand, with ITO negatively biased and carbon foam positively biased during the polarization process. So, the n-doped region can be probed with photoluminescence spectroscopy. Figure 18b shows the photoluminescence spectra measured at 77 K. The results disclose a similar tendency of intensity evolution and peak position shifting (Figure 18c) as Figure 17 a and b when the polarization bias had a different polarity (ITO positive, and carbon foam negative). However, the PL intensity decreased by a much smaller magnitude after 1 V and 2 V polarization; and the peak position blue-shifting was also less significant compared to the results in Figure 17 a and b. This observation suggests n-type doping was not as significant as p-type doping especially after 1 V or 2 V polarization. This is likely due to the size effects and ionic mobility differences of cations and anions of $MAPbBr_3$. Bromine anions can migrate much faster than the methylammonium cations, thus leading to a more significant p-doping than n-doping especially at a relatively low polarization bias.

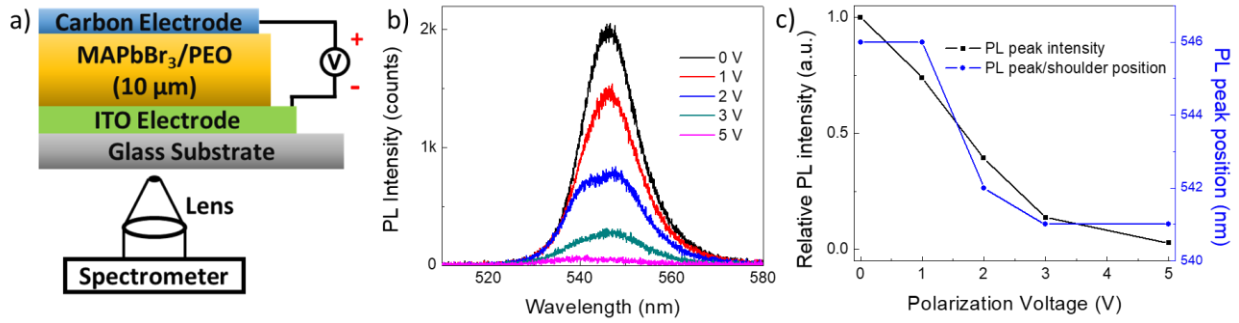

Figure 18. *a) the experimental setup to measure the photoluminescence spectra of the composite film, b) photoluminescence spectra measured at 77 K, c) a summary of PL intensity and peak position of the composite film after each polarization at different voltages (manuscript submitted).*

The ion migration and junction formation in halide perovskite appear like the operation mechanism of polymer light-emitting electrochemical cells (PLECs), a type of single-layer polymer-based electroluminescent device that was first reported by Dr. Qibing Pei and Dr. Alan Heeger in 1995. In PLECs, the emissive layer consists of a light-emitting conjugated polymer admixed with an ionic conductor and a salt. When an external bias is applied, the cations and anions from the salt migrate towards the cathode and anode, resulting in n-type and p-type doping of the conjugated polymer at the cathode/polymer and anode/polymer interfaces, respectively. To further understand the fundamental differences between halide perovskites and ion-containing

conjugated polymers, control experiments were carried out as shown in Figure 19a. A polyphenylene vinylene (PPV)-based yellow-emitting conjugated polymer, super yellow (SY), was used. The SY polymer was mixed with PEO and lithium trifluoromethanesulfonate (LiTf) in tetrahydrofuran (THF) and drop-casted a film on an ITO substrate. The film thickness was about 10 μm. Like measurements in Figure 18, the SY/PEO/LiTf composite film was polarized with a desired bias at 300 K for one minute and then cooled down to 150 K for PL measurements. For the polarization process, the ITO was connected as positive (+); either laminated carbon foam or thermally evaporated aluminum film was connected as negative (-).

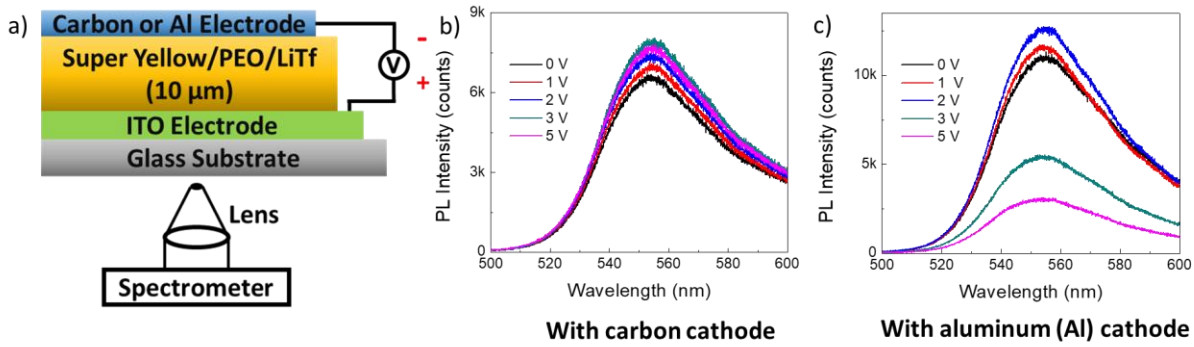

Figure 19. *a) the experimental setup to measure the photoluminescence spectra of the SY/PEO/LiTf film, b) photoluminescence spectra measured when carbon foam was used as the cathode and c) when aluminum was used as the cathode. All spectra were collected at 150 K (manuscript submitted).*

When carbon foam was used as cathode (Figure 19b), the PL intensity of the SY/PEO/LiTf composite film exhibits an increase tendency with increasing polarization voltage from 1 V to 3 V. The PL intensity slightly decreased when the polarization voltage went up to 5 V, but still about 16% higher than the pristine film. It has been known that the PL yield goes down if the conjugated polymer becomes doped. In this regard, the SY polymer was not doped even with a 5 V polarization voltage. The PL intensity increases after each polarization are likely due to ion accumulation effect at the SY/electrode interfaces that makes the main body of SY polymer of higher purity and higher luminescent yield. It is worth to mention that the whole structure of ITO(+)/SY composite/Carbon(-) did emit light with 3 V bias at 300 K, but no light emission with 10 V at 150 K and after 5 V polarization. This observation indicates electrical double layers formed

by ion migration/accumulation can serve to lower energy barriers of charge carrier injection at room temperature, however this mechanism won't work at 150 K due to loss of ionic mobility.

When aluminum was used as cathode (Figure 19c), the PL intensity showed an increasing trend after the film was polarized at 1 V or 2 V. However, the intensity went down by more than 50% after 3 V polarization, and further reduced after 5 V polarization. It is believed the changes of PL intensity after 1 V or 2 V polarization were caused by the ion migration/accumulation mechanism, and by a doping effect after the 3 V and 5 V polarization. The whole structure of ITO(+)/SY composite/Aluminum(-) emitted light with 3 V bias at 300 K. It also emitted light with 3 V bias at 150 K after 5 V polarization. Although both doped polymer and electrical double layers can lower energy barriers of charge carrier injection at room temperature, only doped polymer is effective at 150 K when ion movement has been frozen.

At this point, it becomes clear that ion migration alone not necessarily introduces doping in a conjugated polymer. Doping seems only occurring when the applied bias is over the bandgap of the polymer (2.1-2.2 eV for SY) and when a low work function cathode is used. This phenomenon is distinct from what occurs in halide perovskites. In perovskites, ion migration is accompanied with doping and both n-type and p-type doping can occur at a bias much lower than the E_g/e of the perovskite regardless of electrode work function.

3.2 the junction is not static; it is a propagating one

We also investigated the junction formation process with AC impedance spectroscopy using a device structure as ITO/perovskite composite/In-Ga. The $MAPbBr_3$/PEO composite film was first biased for one minute with a desired DC bias, then immediately switched to an AC bias (100 mV) with a frequency range from 1 MHz to 100 Hz for impedance measurements. As shown in Figure 20a, the Nyquist plots exhibited an arc region within intermediate frequencies that corresponds to the charge transfer processes between the electrodes and the perovskite composite film. The arc portion of the impedance spectra can be simulated using a simplified Randles circuit as shown in Figure 20b. The R_s represents a series resistance of the device, R_{ct} is the total contact resistance quantifying the charge transfer process between the electrodes and the perovskite film, and C is the capacitance. Thus, the following equations 4 and 5 can be used to simulate the experimental data in Figure 20a, where f is frequency.

$$Z_{re} = R_s + \frac{R_{ct}}{1+(2\pi f)^2 R_{ct}^2 C^2} \qquad (4)$$

$$|Z_{im}| = \frac{2\pi f R_{ct}^2 C}{1+(2\pi f)^2 R_{ct}^2 C^2} \qquad (5)$$

The dotted lines in Figure 20a show the simulation results using the R_{ct}, R_s, and C values in Figure 20c. The R_{ct} exhibits a decreasing trend when going from the pristine, to the 5 V biased and then the 10 V biased device. Such results indicate the charge transfer process had been greatly improved after the 5 V or 10 V biasing. This observation is in support of the junction formation fact as previously discussed.

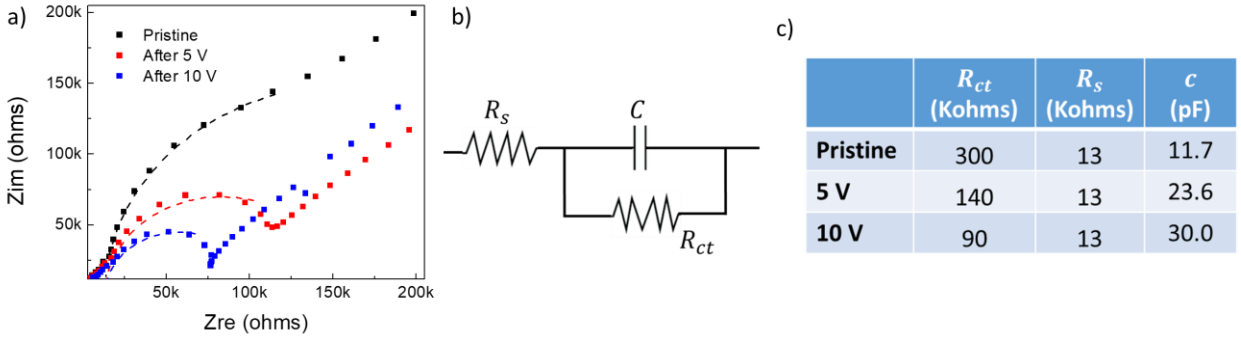

	R_{ct} (Kohms)	R_s (Kohms)	c (pF)
Pristine	300	13	11.7
5 V	140	13	23.6
10 V	90	13	30.0

Figure 20. *a) Nyquist plots of impedance measurements for the pristine device, and after biased it at 5 V and 10 V, respectively. b) A simplified Randles circuit model for simulating the arc regions of the impedance spectra in Figure 20a. Experimental data in Figure 20a are shown as discrete squares, and the dotted lines represent simulation results using the Randles model for the arc regions. c) Summary of the contact resistance (R_{cl}), series resistance (R_s), and capacitance (c) following the Randles circuit model for the pristine device, and after 5 V and 10 V biasing.*

It is noted the capacitance of the perovskite film increased by 100 % after biased at 5 V and 156 % after 10 V, respectively, compared to the pristine film. The solid-state ITO/perovskite composite/In-Ga device can be approximately viewed as a parallel plate capacitor. From the capacitance data, it is estimated the thickness of the intrinsic perovskite layer shrunk by 50% in the 5 V biased device and by 61 % in the 10 V biased device. This result indicates the p-doped and n-doped regions can propagate towards the intrinsic region with an increasing electrical field to reduce the portion of the intrinsic layer.

Considering this junction propagation, it was speculated the original intrinsic layer could eventually disappear, and the p- and n- doped regions may even protrude into the opposite region(s) at a high bias or with a long biasing time. Such a hypothesis explains the relatively short lifetime of all reported halide perovskite LEDs. To verify this hypothesis, we investigated the temperature dependence of the ion migration process and its impact on LED lifetime. The relative current-voltage, and relative luminance-voltage characteristics of $MAPbBr_3$/PEO LEDs were measured at different temperatures as shown in Figure 21 a, b. The device had no polarization history before the measurements.

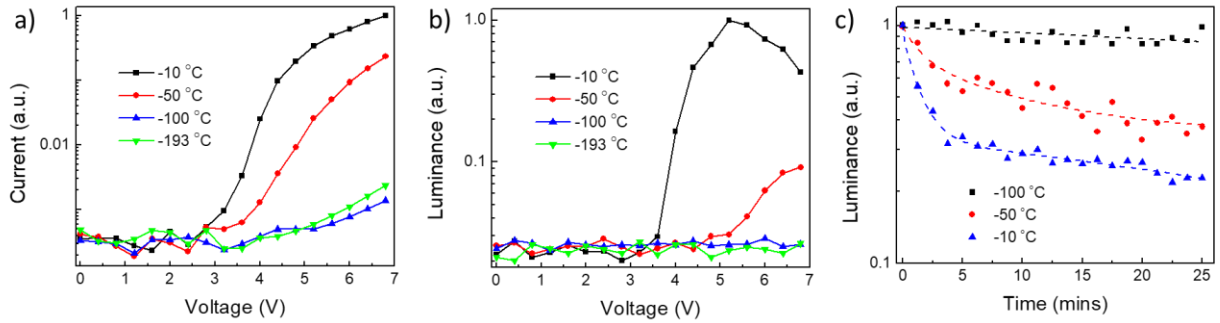

Figure 21. *a) Relative Current-Voltage, and b) Luminance-Voltage of pristine $MAPbBr_3$ LEDs measured at different temperatures. The device had no poling history and measurements started at -193 °C. c) Luminance vs. time studies of $MAPbBr_3$ LEDs at -10 °C, -50 °C, and -100 °C.*

It was seen that the devices exhibited much lower current and no light emission up to a 7 V bias when the temperature was at -100 °C or -193 °C. Such findings suggest the ions became immobilized and no p-i-n junction was formed at or below -100 °C. The operation stability of the LEDs at different temperatures was also compared. For such a comparison, the LEDs were first polarized at 4 V at room temperature, cooled down to a desired temperature with the polarization voltage, and light-emitting intensities were monitored with time. As shown in Figure 21c, the devices appeared very unstable at both -10 °C and -50 °C. However, a substantial improvement was observed at -100 °C. Such temperature dependence of device stability coincides with the temperature dependence of ion migration. Thus, we believe the ion migration and junction propagation is the dominant failure mechanism in perovskite LEDs.

3.3 role of polymer on the ion migration process in perovskites

Ionic conductivity is critical for the ion to migrate and junction to form in perovskite. In a polycrystalline thin film, the ion migration pathways will be dominated by grain boundaries due to the high density of crystalline defects in these regions. In this regard, the choice of polymer will have a high impact on the ionic mobility and thus the degree of ion migration and junction formation in the perovskite/polymer composite films. We have previously used PEO in our perovskite LED demonstrations since PEO is a well-known ionic conductor.

To test that PEO facilitates the migration of the ionic species, control samples were prepared with the PEO replaced by a poor ionic conductor (polyvinylidene difluoride, PVDF) or an ionic insulating polymer (polystyrene, PS). Impedance spectroscopy was used to investigate the ionic conductivity of the $MAPbBr_3$/polymer composites. Figure 22a presents the Nyquist plots for all three samples, demonstrating that the ionic conductivity of $MAPbBr_3$/PEO ~50,000 times higher than the $MAPbBr_3$/PVDF composite. The ionic conductivity of the $MAPbBr_3$/PS composite was too low to measure with the available equipment.

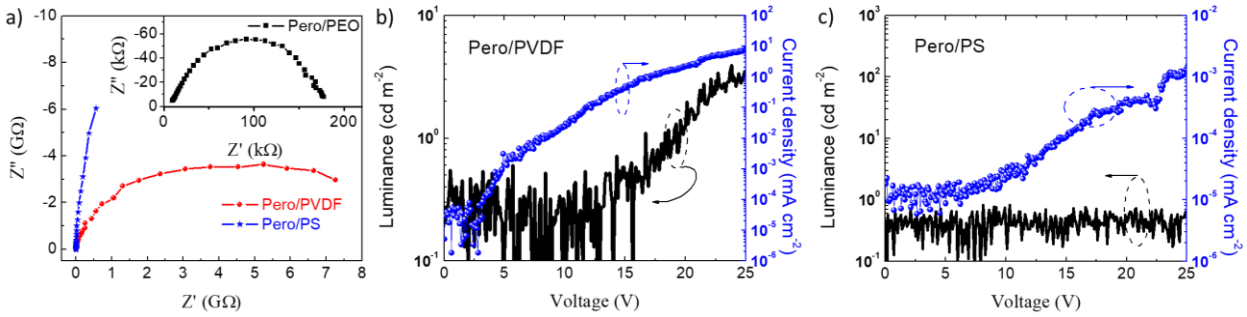

Figure 22. *a) Nyquist plots from impedance measurements of composite films of $MAPbBr_3$/PEO, $MAPbBr_3$/PVDF, or $MAPbBr_3$/PS. b) Current density and Luminance versus Voltage characteristics of LED devices with $MAPbBr_3$/PVDF and c) $MAPbBr_3$/PS composite thin films. The LEDs have a device structure of "ITO anode/perovskite-polymer composite/In-Ga cathode".*

The current density-voltage and corresponding luminance-voltage characteristics of the $MAPbBr_3$/PVDF and $MAPbBr_3$/PS composite devices are shown in Figure 22 b and c, respectively. The $MAPbBr_3$/PVDF composite device turns on at ~19V (1 cd m^{-2}) and reaches ~4 cd m^{-2} at 25V. For the $MAPbBr_3$/PS composite device no luminance could be detected even when the voltage increased to 25 V. The current densities in the PVDF and PS devices were also a few orders of magnitude lower than the PEO device. To this end, the PEO clearly improves the ionic

conductivity of the composite thin film, which contributes to the low driving voltage and high brightness in the single-layer $MAPbBr_3$ LEDs as previously discussed in thrust 1 and 2.

3.4 ion migration in perovskite single crystals

It was discovered the in-situ formed junction due to ion migration can also be utilized to facilitate electronic charge transport in perovskite single crystals. The observation was made using the experimental setup shown in Figure 23a.

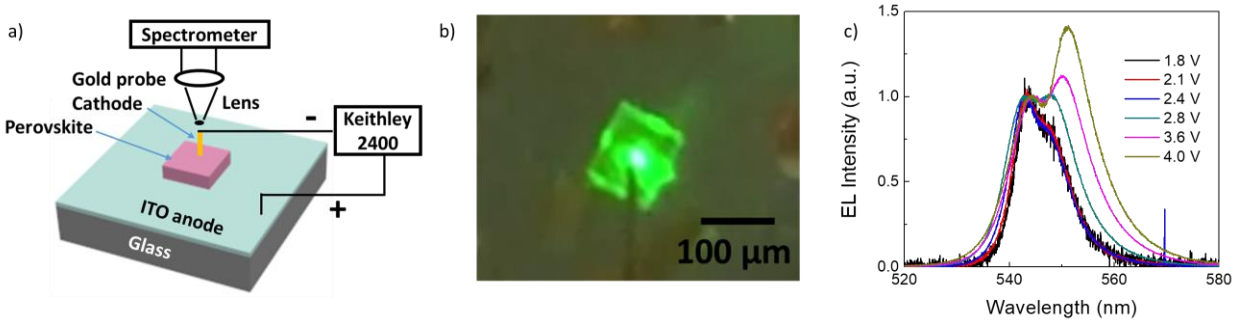

Figure 23. *a) a device model to study the ion migration and junction formation in single crystalline $MAPbBr_3$ microplatelets. b) A photo one lit microplatelet showing intense and whispering-gallery-mode emission at 6 V. c) The electroluminescence spectra of a lit microplatelet at various applied voltages.*

A $MAPbBr_3$ microplatelet was biased at 6 V at ambient temperature, then cooled to 77 K. As shown in Figure 23 b, intense light emission from middle of all the four side surfaces was observed at 77 K. Such a periodic emission pattern was caused by a whispering gallery mode cavity that is formed by the four side-faces of the perovskite crystal. Two peaks can be identified in the electroluminescence spectra of the LED as shown in Figure 23c, one at 542-544 nm and the 2^{nd} at 548-551 nm, attributed to the exciton-exciton scattering processes in the perovskite crystals. The relative intensity of the 548-551 nm peak was enhanced with increasing voltage after 2.4 V, indicating the exciton-exciton scattering process had become more significant at a high injection density of electric charge carriers. A slight red-shifting trend was also observed for the 2^{nd} emission peak after 2.8 V, due to enhanced exciton-exciton scattering at high exciton population.

It is worth mentioning that exciton-exciton scattering can be used as a mechanism to realize stimulated light emission at a low excitation threshold. The whispering gallery mode cavity formed by the smooth outer surfaces and sharp edges and the exciton-exciton interaction in the perovskite

microplatelet crystals can be potentially useful for achieving electrically-driven laser diodes based on perovskite semiconductors.

3.5 electrochemical doping of perovskites with external ion intercalation

The junction formed through ion migration is not static. It only exists when a bias is applied and will disappear when the bias is removed. To obtain a static doping of perovskites, we explored for the first time an electrochemical doping method to controllably form a thin layer of doped halide perovskites on top of an intrinsic perovskite crystal. In general, electrochemical doping utilizes an external bias to reduce (n-dope) or oxidize (p-dope) the semiconductors in an electrolyte environment. Excess charge carriers are formed, accompanied by the insertion of cations or anions to maintain overall charge neutrality in the doped semiconductors.

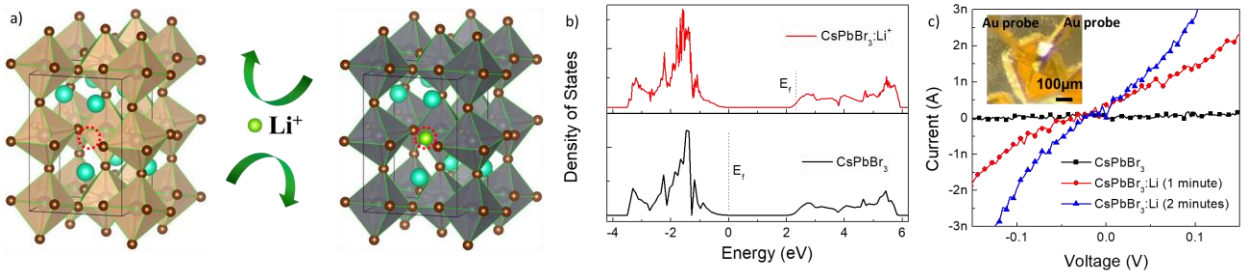

Figure 24. *a) A crystal model shows the lithium ion inercalation to occupy the octahedral interstitial sites in the $CsPbBr_3$ unit cell. b) Density of state (DOS) calculation for the intrinsic (black) and lithium ion intercalated (red) $CsPbBr_3$. c) I-V measurements of isolated $CsPbBr_3$ micro crystals before (black) and after (red and blue) lithium ion intercalation. The $CsPbBr_3$:Li samples were electrochemically reduced at -5 V for one or two minutes in a lithium salt electrolyte. Inset in a) shows the experimental setup for the I-V measurements. Two gold (Au) probes were used to make electrical contacts on the $CsPbBr_3$ micro crystals.*

As a proof of concept, $CsPbBr_3$ was first used as a model perovskite compound for the electrochemical doping study. Before experimental work, DOS calculations based on Density Functional Theory (DFT) were used to investigate how the lithium ion intercalation changed the electronic properties of the perovskites. Due to its lowest formation energy, lithium ions preferentially occupied the octahedral interstitial sites over the substitutional and tetrahedral interstitial sites in the $CsPbBr_3$ lattice ($CsPbBr_3$:Li), Figure 24a. In our calculation, we adopted a configuration of four unit cells (2 × 2 × 1) with one lithium ion. As shown in Figure 24b, the

$CsPbBr_3$ and $CsPbBr_3$:Li exhibit very similar DOS spectra with an energy bandgap of 2.15 eV. The calculated bandgap is close to the reported experimental value. However, the Fermi level (E_f) in $CsPbBr_3$:Li has moved into the conduction band. The result suggests lithium is a donor type impurity for $CsPbBr_3$ and can potentially cause n-type doping to $CsPbBr_3$.

The lithium ion doping effect was verified by current-voltage (I-V) measurements. For such experiments, isolated $CsPbBr_3$ crystals were formed on ITO/glass sbustrates. Two gold (Au) wires with a diameter of 50 μm each were used to make electrical contacts on the top surface of the perovskite crystal (Figure 24c inset). The distance between the two contacts were about 200 μm. The undoped $CsPbBr_3$ crystal showed a background current at ~10 pA from -0.15 V to 0.15 V (Figure 24c, black line). In contrast, the currents from the two lithium ion doped $CsPbBr_3$ samples were significantly larger (Figure 24c, red and blue lines). The improved current can be attributed to a reduced energy barrier between the Au and perovskite, and a higher electrical conductivity in the perovskite after the doping.

We continued investigating the transport characteristic of the lithium ion doped $CsPbBr_3$ for perovskite LED devices. The doped material was employed as an ETL between a high work function gold cathode and an intrinsic $CsPbBr_3$ emissive layer. ITO was connected as the anode, and a gold probe in contact with the $CsPbBr_3$ micro crystal top surface was connected as the cathode of the LEDs. The $CsPbBr_3$ micro crystals were formed on the ITO/glass substrate with thickness of 10-20 μm. The doped perovskite layer was formed by partially reducing the top surface of the micro crystals in a lithium salt electrolyte.

For LEDs with a doped $CsPbBr_3$ ETL, visible light emission was observed at 1.8-2 V in a dark room. At 3.5 V, its emission was intense enough to be clearly visible even in a well illuminated laboratory. This is a very high intensity since the crystals are very small. In comparison, the device without the doped $CsPbBr_3$ ETL ocasionally emitted very dim light at 20-25 V in some $CsPbBr_3$ crystals that were able to sustain such a high bias. At this point, it is worth to mention again that $MAPbBr_3$ crystals can be easily lit up with a low turn-on voltage. The difference between $CsPbBr_3$ and $MAPbBr_3$ can be caused from a higher ionic bonding strength and a relatively lower concentration and moblity of free ions at room temperature in $CsPbBr_3$.

The source of lithium ions for the electrochemical doping can be versatile and the lithium ion doping can be applied to other perovskites. It was also discovered that electrochemical doping

occurred in a sodium ion containing electrolyte, however, not with a potassium or cesium ion-based electrolyte, in agreement with a size limit of ion intercalation that should not exceed the volume of the perovskite interstitial sites.

IV. Some thoughts for future studies

4.1 manipulate ion migration in perovskite composites and single crystals

With the fundamental understanding of using polymers to alter perovskite morphology and ion conductivity, the PI hopes to further the work with the aim to manipulate ion migration in perovskite/polymer composites. The work will involve the synthesis of new ionic conductors that have a high ionic conductivity and can be switched to a low ionic conductivity state through external stimuli.

In our observations, polymers with a high ionic conductivity can facilitate ion migration and junction formation that leads to a low turn-on voltage and a high-power efficiency in perovskite LEDs. Since the junction is of dynamic nature: it forms with an external bias and disappears when the bias is removed. Such a junction won't be ideal for solar cells or many other optoelectronics in which a static junction is typically demanded. Moreover, the propagation of the junction reduces the lifetime of perovskite LEDs. The new ionic conductors will solve these problems and lead to a static and stable p-i-n junction in perovskite/polymer composite films by electrical biasing.

The ion migration can also be manipulated in perovskite single crystals. As previously discussed, $MAPbBr_3$ has a much higher ion mobility than $CsPbBr_3$. Growth of mixed-cation (MA^+/Cs^+) perovskite crystals will allow testing of ion migration and junction formation of single crystals, and their temperature dependency across a large range of ionic mobility/concentration.

2D and 2D/3D layered (Ruddlesden-Popper phase) perovskites have recently demonstrated their effectiveness in improving solar cell stability. The role of ion migration in such materials has not yet been systematically studied, especially how the structural derivation of the organic linkers will impact the ion migration and junction formation process.

Ion migration in perovskites has been treated as a roadblock in perovskite optoelectronics. In the PI's point of view, it brings a unique opportunity of doping and junction formation under a low electrical bias/field that is not possessed by other semiconductor materials. The above

proposed studies will lead to fundamental understanding of the structure-property relationships for manipulating ion migration and aid the search for ideal perovskites or composites that decouple ionic and electrical charge transport processes.

4.2 Electrochemical p-doping of perovskites and electrochemical doping of Ruddlesden-Popper perovskites

Preliminary DFT calculation has shown F^- can be an acceptor-type dopant for $CsPbBr_3$ (Figure 25). The theoretical calculation was done with the PI's collaborator, Prof. Xu Zhang at California State University Northridge. In addition, the ionic radius of F^- is very close to Na^+. It has been observed in our experiment that Na^+ can be electrochemically intercalated into the interstitial sites of the $CsPbBr_3$ lattice. Therefore, it is speculated that F^- will be intercalated at a positive potential. With the readiness of both n- and p-doped perovskites, fundamental studies can be carried out to investigate the effectiveness of p-i-n homojunction on electron/hole injection or collection in perovskite optoelectronics.

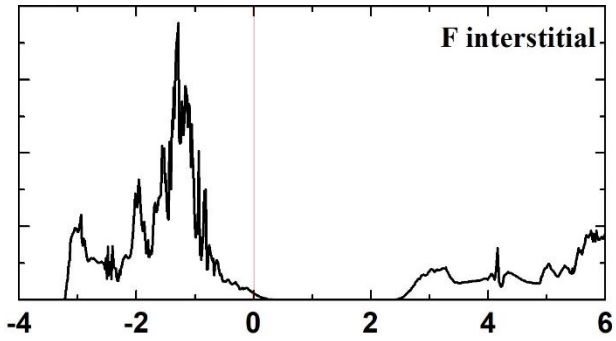

Figure 25. *DOS calculation for fluorine ion intercalated CsPbBr3, suggesting the Fermi level (Ef) in $CsPbBr_3$:F has moved into the valence band to cause p-type doping to $CsPbBr_3$.*

Doping of perovskites into p-type and n-type has been a challenge using the chemical doping method. For instance, charge transfer complex molecules have been recently used by two NREL scientists (Dr. Joseph Luther and Jeffrey Blackburn) to dope perovskite quantum dots. Nonetheless, such molecules will not intercalate perovskite lattices due to their large molecular sizes; moreover, their doping stability can be a concern given the lessens of using such molecules to dope organic and polymer semiconductors.

We also plan to investigate electrochemical doping of Ruddlesden-Popper perovskites. One hypothesis is that their layered crystal structures can potentially tolerate larger size cations

and anions as dopants, thus broadening the dopant material choices to obtain versatile electronic and optical properties of the doped perovskites. We will continue to collaborate with Prof. Xu Zhang at California State University Northridge to seek theoretical guidance for the planed experimental tasks. We will also collaborate with Prof. He Wang at Miami University to measure and understand the photophysical processes of the doped perovskites using femtosecond transient absorption spectroscopy.

Journal publications

1. Li J., Shan X., Bade S. G. R., Geske T., Jiang Q., Yang X., Yu Z.*, "Single-Layer Halide Perovskite Light-Emitting Diodes with Sub- Band Gap Turn-On Voltage and High Brightness", ***Journal of Physical Chemistry Letters***, 7 (30), 4059-4066, 2016.
2. Jiang Q., Chen M., Li J., Wang M., Zeng X., Besara T., Lu J., Xin Y., Shan X., Pan B., Wang C., Lin S., Siegrist T., Xiao Q., Yu Z.*, "Electrochemical Doping of Halide Perovskites with Ion Intercalation", ***ACS Nano***, 11 (1), 1073-1079, 2017.
3. Shan X., Li J., Chen M., Geske T., Bade S. G. R., Yu Z.*, "Junction Propagation in Organometal Halide Perovskite-Polymer Composite Thin Films", ***Journal of Physical Chemistry Letters***, 8 (11), 2412-2419, 2017.
4. Geske T., Li J., Worden M., Shan X., Chen M., Bade S. G. R., Yu Z.*, "Deterministic Nucleation for Halide Perovskite Thin Films with Large and Uniform Grains", ***Advanced Functional Materials***, 27 (40), 1702180, 2017.
5. Chen M., Shan X., Geske T., Li J., Yu Z.*, "Manipulating Ion Migration for Highly Stable Light-Emitting Diodes with Single-Crystalline Organometal Halide Perovskite Microplatelets", ***ACS Nano***, 11 (6), 6312-6318, 2017.
6. Bade S. G. R., Shan X., Hoang P. T., Li J., Geske T., Cai L., Pei Q., Wang C., Yu Z.*, "Stretchable Light-Emitting Diodes with Organometal Halide Perovskite-Polymer Composite Emitters", ***Advanced Materials***, 29 (23), 1607053, 2017.
7. Li, H. R., Shan, X., Neu, J. N., Geske, T., Davis, M., Mao, P. S., Xiao, K., Siegrist, T., & Yu, Z.*, "Lead-free halide double perovskite-polymer composites for flexible X-ray imaging", ***Journal of Materials Chemistry C***, 6 (44), 11961-11967, 2018.

8. Shan, X., Zhang, S. L., Zhou, M., Geske, T., Davis, M., Hao, A., Wang, H., & Yu, Z*, "Porous Halide Perovskite-Polymer Nanocomposites for Explosive Detection with a High Sensitivity", ***Advanced Materials Interfaces***, 6 (3), 1801686, 2019.

Patent applications:

1. Yu, Z., Shan, X., & Li, H. (2019). Halide Perovskite-Polymer Composites and Their Manufacturing Methods for High Energy Photon Detection.
2. Yu, Z., Bade, G. & Geske, T. (2018). Halide Perovskite Thin Films and Methods of Production Thereof.

Outreach and student mentoring

The PI's group had presented their high brightness perovskite/polymer LEDs to groups of visitors in open-house and summer camp at the High-Performance Materials Institute, FSU. Through this project, the PI has sponsored ten undergraduate students and one high school teacher from Puerto Rico for research internships within the past three years. One undergraduate student, one master student and four doctoral students have also been fully or partially sponsored for degree thesis. The undergraduate student won the DOD-SMART Scholarship in 2016 and graduated summa cum laude in May 2018. She is hired by Marine Corps Systems Command. The master student graduated in August 2016 and is hired as a research scientist by eMagin Corporation (an OLED company focusing on commercializing micro LEDs for virtual reality headsets). Two doctoral students graduated in December 2018. One of them is hired as a research scientist by Northrop Grumman and the other is hired as a research scientist by First Solar, Inc.